

Contents lists available at ScienceDirect

# Journal of the Mechanics and Physics of Solids

journal homepage: www.elsevier.com/locate/jmps





# In-operando spectroscopic interrogation of macromolecular conformational changes in polyurea elastomers under high strain rate loading

Nha Uyen Huynh, George Youssef

Experimental Mechanics Laboratory, Mechanical Engineering Department, San Diego State University, 5500 Campanile Drive, San Diego, CA, USA

#### ARTICLE INFO

Keywords:
Spectro-mechanical
Polyurea
Laser-induced shock wave loading
High strain rate
Terahertz spectroscopy

#### ABSTRACT

Temporary and permanent macromolecular conformational changes can accompany the deformation of elastomers under high strain rate loading. Mechanical failure can occur as spallation, volumetric cracking, subsurface morphological changes, and plastic deformations. While high strain rate loading has been extensively reported using various loading mechanisms, where the current state-of-the-art relies on cascading failure and spectroscopic analyses after mechanical loading. In recent years, in-situ spectro-mechanical characterization, entailing concurrent spectroscopic interrogation and mechanical loading, has interested the scientific community in avoiding destructive evaluations in favor of noninvasive characterization, preferably during loading. To overcome the current limitations, this paper reported the first in-operando spectromechanical characterization of elastomeric polymers (polyurea is used as a representative material) loaded at high strain rate using bulk terahertz spectroscopy synchronized in real-time with laser-induced shock wave setup. Spectroscopic terahertz signals were collected concurrently with the imposition of shock waves based on the exfoliation of a sacrificial metallic layer using a highenergy laser pulse with nanosecond duration. The shock-loaded samples were also characterized using the scanning electron microscope, revealing signs of plastic deformations and morphological failure throughout the cross-section, including evidence of crazing and vitrification separately. Multifaceted time and frequency domain analyses elucidated the conformational changes, including spectral peak shifting, enhancement, manifestation, and concealment. The time domain analysis leveraged the dynamic time wrapping approach to quantify the temporal disparity between terahertz signals collected from unloaded, during shock, and loaded samples by calculating the Euclidean distances among signal pairs. Microscopy revealed morphological changes that corroborated the terahertz spectral differences at several energy fluences. Finite element analysis was performed to assess the levels of stresses and strains as a function of the energy fluence from focusing the high-energy laser illumination onto the sacrificial energy layer. The stresses at the depths of failure determined using electron microscopy, corresponded to the tensile strength of the material. The present results demonstrate the viability of the spectro-mechanical characterization of polymers using terahertz-based spectroscopy and laser-induced shock wave, contributing to a new experimental paradigm in polymer mechanics under shock loading.

E-mail address: gyoussef@sdsu.edu (G. Youssef).

<sup>\*</sup> Corresponding author.

#### 1. Introduction

The interactions between intensified shock waves and materials fascinated the materials science and engineering community for several decades, with a renewed interest in the interplay of shock waves with soft matter, including polymers and biological materials (Losego et al., 2012; Grady et al., 2014b; Grady et al., 2014a; Clifton et al., 2016; Grujicic et al., 2015; Malhotra et al., 2021; Albrecht et al., 2013; Lee et al., 2020; Wang et al., 2002; Youssef and Gupta, 2012; G. Youssef and Gupta, 2012). The emphasis on soft materials, in general, stems from their foreseen deployments in extreme conditions that are commonly or easily inaccessible for repair or replacement, e.g., space or bio-implants. Such fascination hinges on the tune-ability of the shock attributes to either suppress all inelastic deformation mechanisms, leading to quasi-elastic failure of the material, or instigating plasticity mechanisms such as dislocation nucleation, mobility, and annihilation, polymorphic transformations, or phase transitions (e.g., vitrification), inclusive of all classes of materials (Meyers, 1994; Renganathan et al., 2020; Srivastava et al., 2021; Youssef et al., 2013; Huynh et al., 2022). In the case of quasi-elastic failure, the shock energy is rapidly transferred to the propagating media, tearing the material apart, which manifests in superficial, deep, or complete spallation (also known as shear plug failure), corresponding to the intrinsic strength of the test materials (Huynh et al., 2022). On the other hand, plasticity failures leech the shock energy (Argon, 2013), channeling to a specific or conglomerate of mechanisms based on their energetic costs in balance with the remaining mechanical energy within the propagating stress waves as a function of the sample dimension in the propagation direction. The attenuation and dispersion of the shock energy during propagation also hinge on the material microstructure and properties.

Several experimental setups have been developed to deliver intensified shock waves, simulating hypervelocity impacts in laboratory environments, which can be holistically classified based on the induced strains and strain rates in the tested material or structure (Meyers, 1994; Ehsani et al., 2021; Shukla et al., 2010; Bourne, 2016; Field et al., 2004; Graziano et al., 2021). Charge detonation has been used to release high speed (> 1400 m/s) and amplitude, in the order of 14 GPa, sound waves in water and air to investigate underwater structures, for example, revealing insights about fluid-structure interactions (Wanchoo et al., 2021). Armor-piercing projectiles (e.g., bullets) also submit protective plates in ballistic testing, irrespective of the monolithic or multilayer materials (Wang et al., 2013; Nayak et al., 2012), but such an experimental setup is not easily accessible in laboratory settings based on the obvious associated occupational risks. Plate impact, split Hopkinson bar, and laser-induced shock waves are frequently used in laboratory settings to generate shock waves in a broad range of materials, spanning over several decades of strain rates while interrogating different length scales (Wang et al., 2002; Ehsani et al., 2021; Weeks and Ravichandran, 2022b; J. Weeks and Ravichandran, 2022a; Gama et al., 2004; Rittel et al., 2002; Wang et al., 2004; Gupta et al., 1992; Gupta et al., 1990). Split Hopkinson bar experiments have various configurations that can load structural materials in tension, compression, shear, and bending with strain rates of  $10^2$ – $10^5$  s<sup>-1</sup> within 10 s or 100 s of microseconds (Weeks and Ravichandran, 2022b; Ravindran et al., 2017; Ravindran et al., 2020; Ravindran et al., 2016). The plate impact setup can investigate the dynamic response of materials with strain rates ranging between  $10^5$  and  $10^8$  s<sup>-1</sup> with loading durations extending over a few microseconds (Elamin and Varga, 2020). A common characteristic of split Hopkinson bar and plate impact is the relatively large strains associated with the corresponding loading scenario, which may lead to localized self-heating from the intensified strain energy unless isentropic state is achieved (Jiao and Clifton, 2014). On the other hand, the laser-induced stress wave setup can load materials at ultrahigh strain rate, i.e.,  $\dot{\epsilon} > 10^6$ , but at significantly lower strains than other high strain rate techniques (Ehsani et al., 2021). Another glaring advantage of laser-induced shock wave experiments is accelerating scientific investigations, allowing the experimentation of several samples within a short time on the optical bench, e.g., (Huynh et al., 2022), compared to the laborious preparations required for the plate impact experiment. Shock-polymer interactions, with a focus on segmented microstructure polyurea (Barsoum, 2015; Blourchian et al., 2021; Huynh et al., 2023), have been captured by our group, demonstrating several deformation and failure mechanisms using experimental and computational approaches (Huynh et al., 2022; Gamez et al., 2021; Huynh and Youssef, 2022). More generally, a recent topical review authored by Ehsani et al. (2021). summarizes the capabilities and limitations of the laser-induced shock wave experiment.

The diversity of high strain rate testing approaches stems from pursuing either the adhesion or cohesion strength of composite or homogenous structures, respectively. Here, the primary shock attribute is the wavelength of the propagating waves with respect to the spatial dimensions of the constituents. The stress wave loads the sample continuum quasi-statically if the wavelength exceeds its linear dimension in the propagation direction. Alternatively, when the dimension of a sample is wider than the wavelength of the shock wave, the latter dynamically submits the material to high strain rate loading based on its rise time. With an emphasis on the high strain rate conditions, several prominent studies employed laser-induced shock waves to explore the behavior of metals, polymers, ceramics, composites, biological materials, and electronics, reporting the intrinsic strength (Grady et al., 2014b; Grady et al., 2014a; Clifton et al., 2016; Grujicic et al., 2015; Malhotra et al., 2021; Albrecht et al., 2013). Studies using shock loading have uncovered the inherent mechanical behavior of impact-mitigating polymers by observation of spallation and shear failure modes, and, remarkably, plastic deformation (Albrecht et al., 2013; Lee et al., 2020; Wang et al., 2002). Laser-induced shock wave loading has also been used to investigate the interfacial strength of composite joints employed in extreme conditions, where the resulting change in dynamic fracture energy and tensile strength were found to be minimal when exposed to high-humidity and high-temperature conditions (Youssef and Gupta, 2012). In the case of studying biological materials, Navarro et al. studied the disruption of biofilms for wound healing applications (Navarro et al., 2012), while Gupta et al. studied the adhesion performance of dental implants (Nakamura et al., 2007; Shim et al., 2009). Recently, Boyd et al. continued to explore the biofilms and cell adhesion in dental implants using laser-induced shock waves (Boyd et al., 2021; Boyd et al., 2019; Boyd and Grady, 2020). As for electronic materials, the adhesion strength of direct wafer bonding was investigated using laser-induced shock waves, where Youssef et al. demonstrated that the intrinsic adhesion strength using this method is far superior to other conventional approaches (Youssef et al., 2012).

The current state-of-the-art in spectroscopy provides a plethora of information on polymers, including their chemical and

molecular composition, identification of functional and molecular groups, and determination of chemical structure (Klöpffer, 2012; Šuštar et al., 2014; Siesler et al., 2008). However, at regimes higher than infrared such as ultraviolet and X-ray (for X-ray photoelectron spectroscopy, XPS), the energy is detrimental to the integrity of the sample, especially when it is exposed for an extended amount of time (Fadley, 2010). Furthermore, to mediate the degradation of the polymer, testing using XPS requires monitoring and reduction of the probing time, limiting the utility of this technique for in-situ or in-operando experimentation. Alternatively, electromagnetic waves within the infrared regime (near, mid, and far-infrared) can generally be used to analytically study the chemical characteristics of polymers nondestructively (Ranby and Rabek, 2012; Smith and Arnold, 2011; Coutaz et al., 2018). For example, Fourier transform infrared (FTIR) spectroscopy is a recognized, rapid, and non-ionizing spectroscopic technique used to uncover the functional groups of polymers (Koenig, 1984). While this reliable technique has provided insight into the unique spectra of different materials and material systems, the penetration depth is limited to a few microns, i.e., the surface effect (Koenig, 1984). Additionally, FTIR generally operates at absorption frequencies of 400-4000 cm<sup>-1</sup>, which is efficient at discerning functional groups and can, therefore, be used to identify a material. However, the frequencies of the vibrational modes associated with the underlying mechanisms of impact mitigating polymers are found in the terahertz regime (3-300 cm<sup>-1</sup>). Terahertz-based spectroscopy (e.g., terahertz time-domain spectroscopy) has been recently explored to overcome these limitations due to the technological advancements in pulsed femtosecond laser and the detection of terahertz waves (Smith and Arnold, 2011; Coutaz et al., 2018). The photon energy of electromagnetic waves less than 6 THz is below that of thermal energy at room temperature; therefore, terahertz waves are also non-ionizing, noninvasive, and nondestructive to polymers (Huynh et al., 2022; Huynh and Youssef, 2022; Smith and Arnold, 2011; Coutaz et al., 2018; Huynh and Youssef, 2021). Moreover, since polymers are highly transparent to terahertz waves, bulk terahertz-based spectroscopy was used to characterize several polymers with a wide range of thicknesses (Smith and Arnold, 2011; Coutaz et al., 2018; Rostami et al., 2010; Nüßler and Jonuscheit, 2021; Cheng et al., 2022).

Therefore, this research aims to characterize the temporal and spectral terahertz changes of polyurea in-operando high strain rate loading using laser-induced shock waves. Polyurea is studied herein since it is a complex representative polymer from the sub-class of elastomers with segmented microstructure comprising of hard and soft segments (Barsoum, 2015; Blourchian et al., 2021; Huynh et al., 2023). In addition, simulated results using finite element analysis were used to demonstrate the mechanical behavior of shock-loaded polyurea. The novelty of this research is embodied in the first demonstration of concurrent spectro-mechanical characterization of shock-loaded polymers, detecting molecular structure changes due to intense mechanical loading nondestructively using terahertz-based spectroscopy.

#### 2. Materials and methods

Shock-loaded polyurea samples were concurrently analyzed using terahertz time-domain spectroscopy (THz-TDS) configured in the right-angle reflection mode. The following three subsections are organized to delineate the details of ( $\S$  2.1) the sample preparation of polyurea elastomers, ( $\S$  2.2) the reflection terahertz spectroscopy setup, and ( $\S$  2.3) the laser-induced shock wave loading experimental setup. The latter two setups were synchronized upon releasing the photonic energy from the high-energy laser used to generate shock waves. Notably, the terahertz spectroscopy section ( $\S$  2.2) was augmented by time and frequency domain analyses to exploit the collected data. In addition, the laser-induced shock wave setup section ( $\S$  2.3) was supplemented by finite element simulation to assess the mechanics of polyurea undergoing high strain rate loading.

## 2.1. Sample preparation

The final sample configurations hinged on three experimental considerations, the prime of which is the overarching objective of facilitating concurrent shock loading and spectroscopic characterization. Second is the physical arrangements of the terahertz spectroscopy (§ 2.2) and the laser-induced shock wave (§ 2.3), limiting the placement of the samples with respect to the interrogating terahertz beam and focusing lenses, respectively. Finally, THz-TDS signals were collected from the same spot on the sample before,

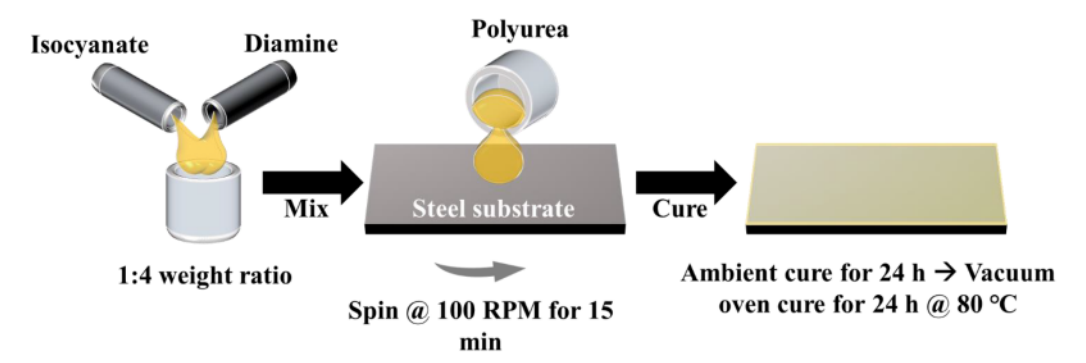


Fig. 1. Sample preparation steps, including mixing isocyanate and diamine at weight ratio of 1:4 for at least 90 s, followed by spin coating the stainless-steel substrate at 100 rpm for 15 min, and curing at ambient and heated, vacuumed conditions. Polyurea was deposited on mirror-finished stainless-steel substrate to enhance the input stress wave and act as a reflective surface for the terahertz interrogating beam.

during, and after the shock loading to probe any conformational changes; hence, constricting the mobility of the sample throughout the measurements was imperative. Each sample consisted of a  $668\pm31$  µm thick polyurea layer and a mirror-finish, 304 stainless-steel substrate with a nominal thickness of 760 µm. Mirror-finished stainless-steel substrates were used to (1) act as a reflective mirror of the terahertz wave and (2) enhance the strength of the shock wave, given its high density and stiffness compared to those of polyurea (recall,  $\sigma_{in} = -\frac{1}{2}\rho cv$ , where  $\rho$  is the density of the substrate, c is the longitudinal wave speed, and v is the shock-induced free surface velocity). The substrates were precut into 76.2 mm long  $\times$  25.4 mm wide strips, which were cleaned before the deposition of polyurea using a 50:50 solution of isopropyl alcohol and deionized water to remove any organic and dust contaminates. As shown in Fig. 1, polyurea mixture was first prepared by thoroughly and slowly mixing an oligomeric diamine (Versalink P1000, Evonik) and a modified isocyanate (MDI 143 L, DOW) at a weight ratio of 4:1 for at least 90 s. The mixture was then deposited on the polished side of the stainless-steel substrate and spin-coated at ambient conditions for 15 min at 100 rpm. The polyurea-coated substrates were cured at ambient conditions for 24 h and then for another 24 h under vacuum at 80 °C. The back side of the stainless-steel was then coated with a ~500 nm silver sacrificial layer using a physical vapor deposition system (Quorum Q150T turbomolecular coater). At least 30 min before shock loading, the silver sacrificial layer was covered by a ~50 µm thick sodium silicate confining layer for the reasons discussed in § 2.3. Fig. 1 schematically summarizes the sample preparation steps. A total of three samples were fabricated and characterized. Each sample was loaded at eight different spots, resulting in 24 individual spots for shock loading.

#### 2.2. Reflective terahertz time-domain spectroscopy (THz-TDS)

This research used a built-in-house THz-TDS setup in a right-angle reflection configuration. A pulsed femtosecond laser beam (Menlo Systems, ELMO 780 HP) was first split into two different paths. In one path, a terahertz beam was generated by focusing the source beam onto an active area of a photoconductive antenna transmitter (PCA, Batop, PCA-40-05-10-800). The collimated, emitted terahertz wave passed through a 50:50 THz beamsplitter and focused onto the polyurea sample. The returning wave reflected off the mirror-finish, stainless-steel substrate to be collimated, orthogonally reflected, and focused onto a receiver PCA (Batop, bPCA-100-05-10-800). On the other hand, the second path was sent to a delay line, using a vibration generator operating at 12.3 mm/s, to

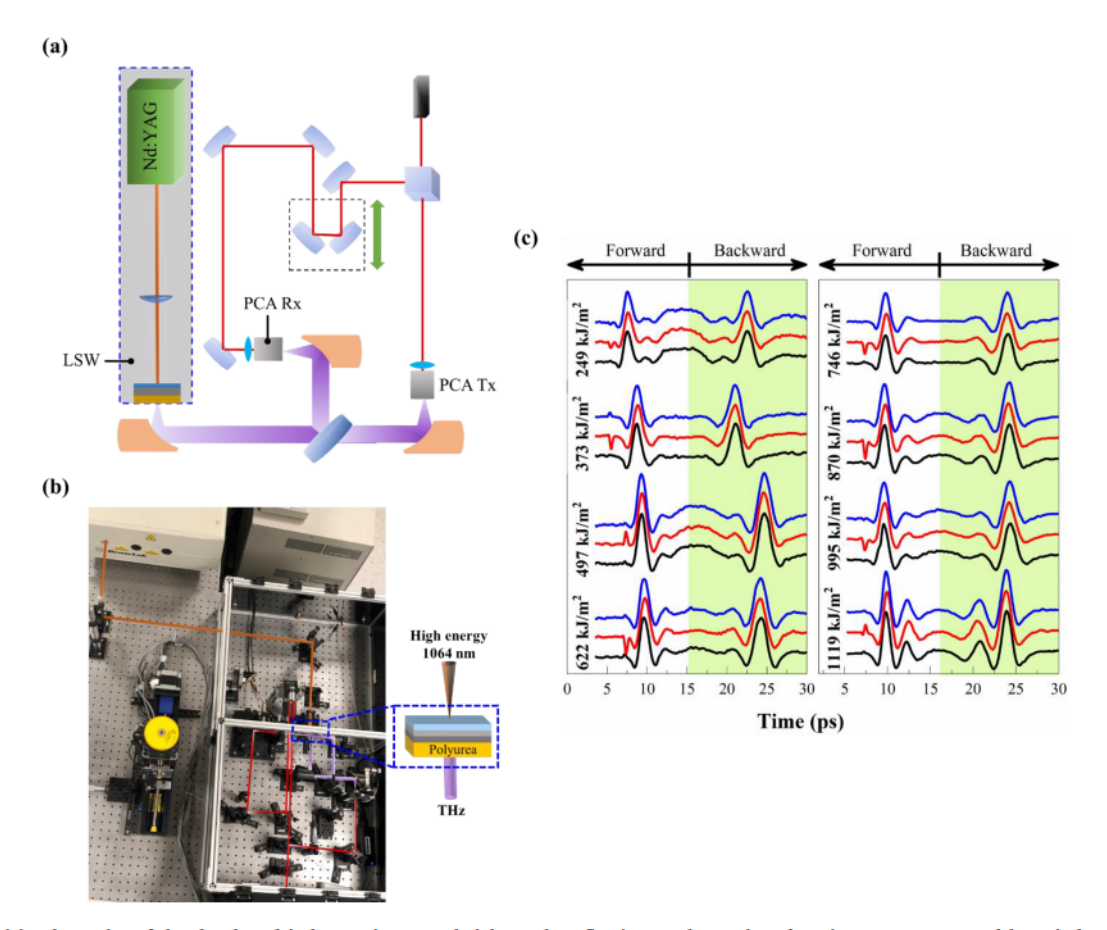


Fig. 2. (a) Schematics of the developed in-house, integrated right-angle reflection terahertz time-domain spectroscopy and laser-induced shock wave setup, (b) the actual in-house setup used to simultaneously shock load at high strain rate and spectroscopically interrogate polyurea elastomer, and (c) the resolved reflected terahertz time-domain signals at eight different energy fluences used to generate laser-induced shock waves, showing the concatenated forward and backward trips of the retroreflector (only forward trips are considered herein).

activate the receiving photoconductive antenna at the same instant the THz wave from the first path arrived at the receiver antenna. The generated photocurrent was converted and amplified into a measurable electrical signal, which was collected using a lock-in amplifier (LIA, Stanford Research Systems, SR830). The signal from the LIA was input into a digitizer (Tektronix DPO 7254) and triggered at 100 mV of the rising edge of a square wave from the high-energy laser upon the firing command. The terahertz time-domain data was recorded of the same spot on the sample before, during, and after shock loading using the same synchronization command. That is to say, three signals were collected at each spot, where each signal was obtained at three distinctive circumstances. The first signal was collected of the virgin unloaded sample (denoted as 'before'), the second signal was collected while the shock wave propagated through the sample thickness (referred to as 'during') based on the trigger command coinciding with the release of the laser energy, and the third signal was collected post shock loading, when the shock wave has completely attenuated (e.g., 'after' loading). The x-axis of the acquired data, i.e., the travel distance of the delay, was converted to the time traveled by the femtosecond beam to yield the time-domain THz data. Mounting the retroreflector on a vibrating stage allowed the acquisition of two THz signals: one of the forward trip and the other during the backward trip. Fig. 2a shows a schematic representation of the THz-TDS setup used in the research leading to this report. Fig. 2c includes the raw time-domain signals at different laser fluences, as discussed next.

As shown in Fig. 2c, comparisons between the before, during, and after signals at any given energy fluence are limited to only qualitative analysis. Hence, the raw time-domain data underwent the following processing steps to signify the effect of shock loading on polyurea while allowing quantitative comparison between the different energy fluences. The following procedure was necessary since cross-correlation of the time-domain signals were proven to be futile. First, the raw data within each energy fluence loading regime were shifted to align the primary peaks of the terahertz signals collected before, during, and after shock imposition. The unloaded signal was used as the reference signal, i.e., the remaining signals were shifted to line up with the primary THz peak of the before-loading signal. Second, a new time domain comparison metric was introduced by calculating the dynamic time wrapping (DTW) between the before  $(x_b(t))$  and during  $(x_d(t))$ , before  $(x_b(t))$  and after  $(x_a(t))$ , and during  $(x_d(t))$  and after  $(x_a(t))$  signals by measuring the sum of the Euclidean distances between the signal pairs. The DTW metric was used since only minute differences were noted between each group of THz signals when comparing the before, during, and after data even after shifting and aligning the peaks. Such minute differences proved the deduction of a trend based on several comparison metrics, including peak width and prominence, to be elusive due to the lack of a common datum linking all the signals together. The dynamic time wrapping metric was calculated using Signal Processing Toolbox in MATLAB® based on the root sum squared differences (also referred to as  $\ell_2$  metric)

$$\ell_2 = \sqrt{\sum_{k=1}^{K} (x_n(t) - x_m(t))^2}$$
 (1)

where, n, m = b, d, or a representing the before, during, and after signals, respectively. The  $\ell_2$  metric quantifies the temporal difference (shift and stretching) for a signal pair to coincide. Given the characteristic differences between the signals (inter and intra energy fluence), the normalized terahertz signal power ( $\mathfrak{E}$ ) was used in lieu of the raw shifted signals, which was calculated as

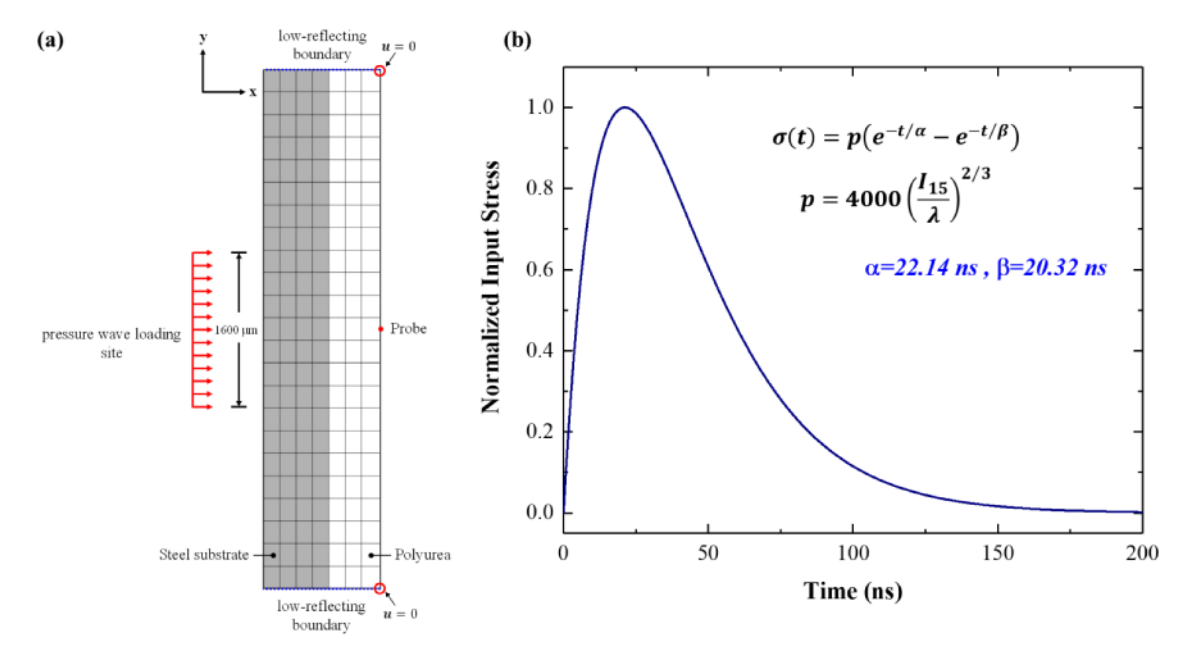


Fig. 3. (a) Schematics of the finite element simulations showing the kinematic and loading boundary conditions while noting the probe used to extract the free surface displacement and velocity at each energy fluence level, and (b) the normalized input stress profile where the amplitude calculated using Lindl's equation was based on the illumination energy. The temporal characteristics of the input stress wave (i.e., values of  $\alpha$  and  $\beta$ ) are based on standalone interferometric measurement off the uncoated stainless steel substrate surface.

$$\mathfrak{E} = [x_n(t)]^2 / \max([x_n(t)]^2). \tag{2}$$

Finally, the shifted and aligned terahertz signal powers were transformed into the frequency domain using the discrete fast Fourier transform, where the frequency-transformed spectra were compared within each energy fluence using the spectral features in the amplitude-frequency plots as a comparative metric.

#### 2.3. Laser-induced shock wave (LSW)

The laser spallation technique was used to mechanically load each polyurea sample at eight different locations with varying energy levels using a high-energy Nd:YAG pulsed laser (Spectra-Physics, Quanta-Ray PRO 350). Fig. 2a and b show the schematic and the physically integrated LSW setup with the terahertz spectroscopy discussed in the previous section, respectively. The loading spots were separated by >10 mm to avoid any stress wave interactions or unintentional preloading through crosstalk. The focused, high-energy Nd:YAG beam of 1.6 mm in diameter interacted with the confined Ag layer (Huynh et al., 2022), which underwent a rapid thermal expansion, launching a localized compressive stress wave towards the polyurea sample. Each spot was loaded at a different laser energy level exactly once to avoid fatigue and suppress any rate- and time-dependent deformation mechanisms. The energy fluences (illumination energy divided by the illumination area based on the spot size) ranged between 249 mJ/mm² to 1119 mJ/mm² at an increment of 124 mJ/mm². Each energy fluences was loaded at three different spots, identified on the three different steel/polyurea samples.

Complementary to experimental observations of shock-loaded polyurea is a finite element analysis (FEA) replicating the stress wave propagation in the stainless-steel substrate and bonded polyurea plug. The details of the FEA analysis of the undertaken problem was recently reported by Gamez et al. (2021), briefly summarized herein based on Fig. 3a schematics. Due to the high strain rate loading conditions, all materials were modeled using linear elasticity based on their wave speeds, as discuss in Gamez et al. (2021). The successful completion of the simulation hinges on the material properties, the applied and prescribed boundary conditions, and spatiotemporal discretization. Fig. 3a also shows the corresponding boundary conditions, including the applied compressive stress wave at the free surface of the substrate, symmetry and low-reflective boundary conditions at the lateral extremities of the geometry; the sample free surface was set to be traction free. The input stress wave was defined based on the normalized profile shown in Fig. 3b and the amplitude was based on the energy fluence and on Lindl's equation (Huynh et al., 2022; Ready, 1965; Ready, 1997). The normalized profile was digitized in accordance with the published experimental study in Youssef and Gupta (2012), Huynh et al. (2022), Gamez et al. (2021), defining the temporal attributes of the normalized stress wave, including the rise and decay times as well as the pulse duration. According to Lindl's equation, the amplitude of laser-induced pressure (P, in GPa) is related to the laser intensity ( $I_{15}$ , in  $I_{15}$ ), in  $I_{10}$ 

$$p = 4000(I_{15}/\lambda)^{2/3} \tag{3}$$

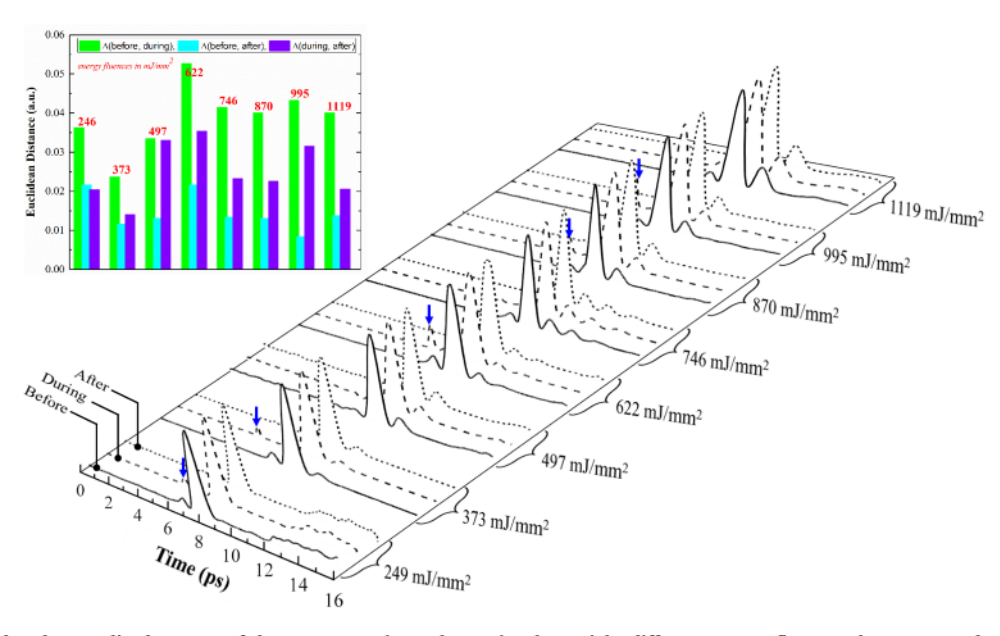


Fig. 4. Shifted and normalized powers of the spectroscopic terahertz signals at eight different energy fluences that were used to generate and propagate compressive stress waves through the substrate/polymer samples. At each energy fluence, a triad signals are stacked resembling the terahertz data collected before, during, and after shock loading. The inset summarizes the sum of the Euclidean distances between before, during, and after shifted terahertz power signals at the same energy fluences used in the experiment.

where,  $\lambda$  is the laser wavelength in  $\mu$ m. In this investigation,  $\lambda = 1.064 \, \mu$ m,  $A = 0.02 \, \text{cm}^2$ ,  $I_{15} = E/A.t$ , with a typical mean rise time (t) of 10 ns (Ready, 1965; Ready, 1997). The utility of Lindl's equation to estimate the stress amplitude based on each energy fluence was favored instead of the usual interferometric approaches, given the obvious experimental limitations of the current study preventing access to the free surface since it was used for spectroscopic measurements. The materials properties and the discretization schema were faithfully replicated based on the recent study by Gamez et al. (2021).

Finally, the changes in the morphology of the cross-section of the shock-loaded samples were captured using a scanning electron microscope (SEM, FEI, Quanta 450). The cross-section was prepared using diamond saw, cutting the samples through the loaded spots. Before placement in the microscope, the surfaces of the steel/polyurea sections were coated with 6 nm of platinum. SEM micrographs were obtained at varying accelerating voltages and working distances.

#### 3. Results and discussion

Fig. 4 shows the resolved THz time-domain data as a function of the high-energy laser fluence used to induce the stress waves at different amplitudes. The figure displays the normalized and shifted THz power of the signals previously presented in Fig. 2c. Three stacked waveforms are included at each energy fluence, representing the resolved THz signals before, during, and after shock loading at the same spot on the sample. As discussed above, each waveform was collected based on the triggering command from the highenergy laser. The laser beam was blocked completely from interacting with the sample when collecting the before and after signals, whereas it was allowed to exfoliate the Ag film and generate a stress wave in the remaining case. Fig. 4 reveals three initial observations, which are discussed qualitatively and explained quantitatively in the forthcoming sections. Generally, the THz signals shown in Fig. 4 consisted of three consecutive peaks, where the main, prominent peak was surrounded by two eclipsed peaks: one preceding and the other following. However, an additional peak manifested in the THz signal concurrently collected during the shock propagation, irrespective of the shock amplitude, marked by the down-arrows in Fig. 4. The inset in Fig. 4 shows the Euclidean distances comparing the before/during, before/after, and during/after signal pairs. Generally, the results illustrate the disparity between these signals collected at the same spot, irrespective of the loading energy fluence. The Euclidean distances between the before and during terahertz signal pairs were consistently higher than the remaining counterparts, signifying the ample required time wrapping to achieve coincidence. A similar trend persisted while overlaying the during and after signal pairs calculating dynamic time wrapping distances. On the other hand, the sum of Euclidean distances between before and after signals were the smallest among other pairs, demonstrating the close resemblance between the terahertz signatures in the unloaded and post-loaded spots. The Euclidean distance differences imply (1) shock-polyurea interaction resulted in dynamic traceable conformational changes, and (2) shock-loaded polyurea underwent molecular and continuum elastic and plastic deformations.

First, while the signals shown in Fig. 4 were shifted for the reasons discussed above, the shifting time delays for each signal pair were calculated during the data post-processing step and plotted in Fig. 5a. The time lag was associated with physical changes in the sample thickness due to the induced strains during the shock propagation. On average, the time delays between the unloaded (before) and after shock-loading (after) signals were 45–74% smaller than those between the before and during shock propagation (during) signal pair. Furthermore, the delays monotonically decreased with the illumination energy at a slope of ~0.008 ps/J and ~0.02 ps/J for before-after and before-during signal pairs, respectively. That is to say, the waveforms before (unloaded sample spot) and after shock loading (same loaded and relaxed sample spot) are nearly coincident, indicating (1) rigid fixation of the sample during testing and (2) shock-induced deformations were approximately reversible. The former implies that all rigid body motions were correctly constrained by clamping the sample in a specially designed holder. The location of the sample with respect to the THz beam path was imperative for the acquisition of reliable spectroscopic time-domain data; when violated, the signal can roam over the time axis with

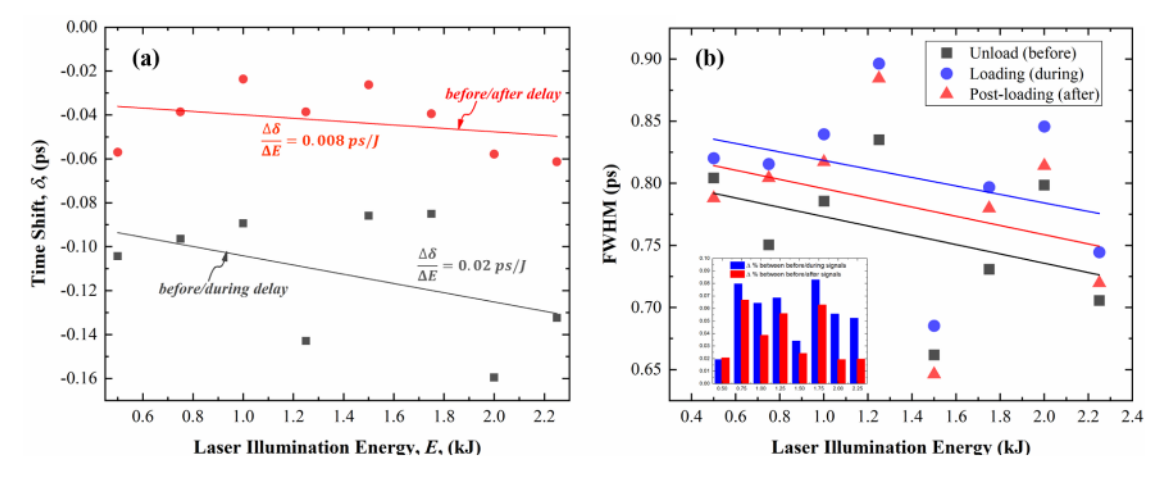


Fig. 5. Average (a) delays between before/during and before/after terahertz signal pairs and (b) full width at half-max (FWHM) of the before, during, and after shock loading terahertz signals. The delays increased while the FWHM narrowed as a function of the laser energy, elucidating molecular structural changes in shock-loaded polyurea.

degraded prominence and broadened spread. As shown in Fig. 2c, the signal amplitude remained nearly unchanged for the signals collected before, during, and after shock loading, implying that the recorded time shifts were most probably due to shock-induced deformations. In other words, the impossibility of jolting the sample from the static equilibrium position was axiomatic based on the near coincidence of the waveforms deduced from the shifting differences. The latter designates that the deformation induced by the propagation of the initial compressive wave and reflected tensile wave was moderately elastic. Any shock-induced plastic deformations were exemplified by the delays between the waveforms, as shown by the difference between delays of before/after and before/during signal pairs. The delays ( $\delta$ ) are prognostic of changes to the real part of the refractive index (n) such that

$$n = 1 + c\delta/d$$
 (4)

where, *c* is the speed of light in vacuum, and *d* is the sample thickness at the interrogation spot (Huynh and Youssef, 2021). To further discuss the changes in the real refractive index, the shock-induced strains must be known *a priori* to account for changes in the sample thickness during shock propagation. This point is explicated in a forthcoming section based on the results of the FEA simulation.

Second is the change in full width at half max (FWHM) of the primary THz peak, where the corresponding averages of before, during, and after signals were collated in Fig. 5b. On average, the peak widths (i.e., FWHM) of the THz signals collected before shock loading were ca. 6% and 3% smaller than those acquired during or after loading, respectively. It is imperative to note that the downtrend in the regressed line through the average FWHM as a function of the energy fluence is circumstantial since it persisted irrespective of the acquisition conditions, i.e., the similar negative slope for the THz signals collected before, during, and after shock loading. Therefore, the data should be intra-compared within each loading regime (energy fluence) since a common reference was not available or feasible. Changes in the FWHM imply evolution in the optical dispersion properties of the material due to morphological changes associated with elastic and plastic deformations from the propagation of the shock wave. The inset in Fig. 5b summarizes the disparity of the FWHM of before/during and before/after signal pairs. Such disparity further exemplifies the previous conclusions about the close resemblance between the THz signals collected from the unloaded sample and that acquired after the plug was loaded and relaxed following the propagation of the shock wave. The disparity between before/after signal pairs was persistently lower than those based on comparing the before/during signal pairs, indicating combined shock-induced elastoplastic deformations since terahertz signal never retreated to its unloaded character. The least significant disparity was reported at the lowest energy fluence of 249 mJ/mm<sup>2</sup>, while the highest was associated with loading the sample with a shock wave resulting from 1119 mJ/mm<sup>2</sup> fluence. In general, the laser-induced shock waves were attributed to underlying structural changes in polyurea as indicated by FWHM and time delays, which are further discussed based on the spectral analysis below.

Finally, and unique to the waveforms collected during the shock wave propagation, is the manifestation of an additional peak leading to the characteristic triad peaks in the terahertz signals, substantiating the concurrency of terahertz acquisition and propagation of the shock waves. The superfluous peak consistently led the primary peak by approximately 2.2–3.5 ps, suggesting it was strongly coupled to the shock-induced stress and deformation states. It is then essential to reiterate that time delays and FWHM confirmed the samples were well constrained, preventing any rigid body motion that may result in unintentional translation of the peaks along the time axis. This peak manifestation was then attributed to the shock wave splitting into the precursor shock wave that

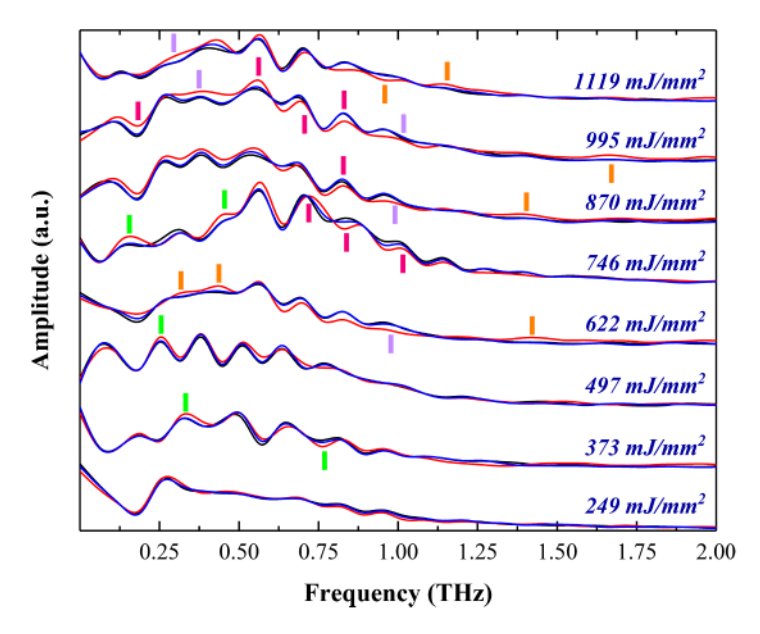


Fig. 6. Spectral amplitude of terahertz signals collected from the same spots of steel/polyurea samples at different energy fluences, ranging from 249 mJ/mm² to 1119 mJ/mm², showing peak enhancement (green marks), shift (red marks), manifestation (orange marks), and concealment (purple marks). The plot also highlights the similarities between the spectra of unloaded (black) and post-loading (blue) spots, exemplifying the dominance of elastic deformation and induction of shock-induced molecular and continuum plasticity.

pushed the polyurea plug beyond its yield point and the compressive plastic wave capable of inducing momentary and permanent entropic changes. The latter is consistent with the previous observations based on changes in delays and FWHM. The levels of stresses and accompanied strains are discussed next based on the results of the FEA simulations at different energy fluences.

Fig. 6 shows the THz spectra results from frequency analysis of the raw data reported in Fig. 2c (only the signal collected during the forward trip of the retroreflector). Given the limited temporal resolution to accommodate the shock-triggered terahertz data acquisition, the spectral bandwidth was bounded up to *ca.* 1.25–1.30 THz, capturing spectral features of the unloaded and loaded polyurea plugs. The spectra bandwidth of the current experimental setup can be further improved in future research using higher acquisition rate electronics. The spectral results in Fig. 6 highlight three essential observations. First, the close spectral resemblance between the amplitude of the THz signal of the unloaded sample and that collected after shock loading, irrespective of the energy fluence, strongly agreeing with the outcomes of the time-domain analysis. The minuscule difference between the amplitude spectra of the terahertz signals collected before and after loading is associated with their similarities in the temporal characteristics between these signal pairs, as discussed above. The slight differences exemplified in all the panels within Fig. 4, especially for energy fluences ≥746 mJ/mm², indicate the extent of shock-induced plastic deformation. In some cases (e.g., signals corresponding to energy fluence of 497 mJ/mm²), the amplitude spectra of the before and after THz signals are indistinguishable, illustrating the underlying recovery of polyurea after shock loading. In other words, polyurea nearly retained its original molecular structure despite the propagation of intense laser-induced shock waves. That is to say, disrupted interchain hydrogen bonds (isocyanate chains) due to shock loading presumably recovered due to the returning tensile wave and the degree of crosslinking in polyurea.

Second is the notable spectral changes in the terahertz signals collected during the propagation of the shock waves, irrespective of the shock amplitude. The terahertz spectral changes recorded during the propagation of the shock waves include peak enhancement, shift, manifestation, or concealment, evidencing momentary molecular changes in the polyurea structure due to its interactions with the shock wave. Peak enhancement is defined as an increase in peak prominence in the spectrum, while peak shift is attributed to the movement of a given peak over the frequency axis. If a peak appears on the spectrum, it is identified as peak manifestation, whereas the opposite is true for peak concealment. For example, spectral peak enhancement was present at 0.32 THz and 0.76 THz for samples loaded with shock waves at an energy fluence of 373 mJ/mm<sup>2</sup>, and 0.25 THz at 497 mJ/mm<sup>2</sup>. Several other peaks were also enhanced, including 0.16 and 0.44 THz for the higher energy fluence of 746 mJ/mm<sup>2</sup>. Such an increase in the amplitude of the spectral peaks, i.e., peak enhancement, is associated with the increased presence of vibrational modes within the frequency context studied herein. Peak shifting was pronounced at several energy fluences, such as the 0.73, 0.82 and 1.02 THz at an energy fluence of 746 mJ/mm<sup>2</sup>. The spectral response also elucidates other shifted peaks, including 0.82 THz at 870 mJ/mm<sup>2</sup>, and 0.19, 0.56, 0.70 and 0.82 THz for the case of 995 mJ/mm<sup>2</sup> energy fluence. In general, peak shift is associated with transferring the vibrational energy at one frequency to a neighboring counterpart, excitation of phantom vibrational mode, or altering the bond orientation with respect the integrating terahertz waves (recall, e = kf, where e is the vibration energy, k is Planck's constant, and f is the frequency). Hence, up-shifting (blueshifting) is attributed to an increase in frequency, while down-shifting (red-shifting) coincides with reducing the vibrational energy for the same molecule. Within the context of vibrational energy, several spectral peaks manifested in the terahertz signals acquired during shock wave propagation based on the excitation of additional molecular vibration modes. For example, two spectral peaks appeared at 0.32 and 0.76 THz in terahertz signals collected concurrently to the propagation of stress waves at the energy fluence of 373 mJ/mm<sup>2</sup>. Additionally, a peak manifested at 0.25 THz for the loading case at 497 mJ/mm<sup>2</sup> and 0.16 THz and 0.44 THz at 746 mJ/mm<sup>2</sup>. Finally, various peaks were concealed within the terahertz spectral responses acquired during shock loading, most prominent at higher energy fluences. At 995 mJ/mm<sup>2</sup>, two spectral peaks at 0.38 and 0.98 THz ebbed in the spectrum of terahertz collected during shock propagation, while 0.32 THz peak receded from the 1119 mJ/mm<sup>2</sup> spectra. As discussed before, polyurea is hallmarked for its segmental structure of hard and soft domains stemming from the chemical constituents, where the hard segments are mechanically enhanced due to the formation of hydrogen bonds. The latter are generally four times weaker than covalent bonds and require proximity between adjacent hard segments in polyurea. Hence, the energy to recreate this type of bond is also energetically favorable. It is hypothesized that peak disappearance, as shown in Fig. 6, is attributed to the shock waves mechanically displacing the hard segments, resulting in momentary dissociation. The dissociated hydrogen bonds reverted either during the returning stress wave from the free surface of the sample or the recovery phase upon load removal. In general, the spectral amplitude of the terahertz signal is linked to changes in the absorption coefficient ( $k \propto \ln(|A|)$ , where A is the spectral amplitude). To pinpoint and ascertain the source of these spectral variations, this research group currently pursues state-of-the-art molecular dynamics and molecular mechanics to couple the effect of mechanical loading at high strain rates with spectral changes in the terahertz regime.

The final observation based on the spectral results shown in Fig. 6 is the coupling between the intensity of the shock waves and spectral changes in the terahertz regime. At low energy fluences (e.g., < 497 mJ/mm²), the spectral responses generally exhibited similar features, where the frequency response of terahertz signals collected before, during, and after shock loading were in good coincidence. On the other hand, the spectral deviations reported above, including peak enhancement, shift, manifestation, or concealment, corresponded to shock loading at higher energy fluences (e.g., > 622 mJ/mm²). This is because the input mechanical energy due to shock propagation at high strain rate disrupts the molecular structure of polyurea instantaneously, where an increase in the shock amplitude due to a rise in the energy fluence perturbs the macromolecule, allowing terahertz probing. This final outcome demonstrates the first report about the significance of terahertz spectroscopy as an approach for in-operando and in-situ characterization of polymers under shock loading.

In a prior report, Zhao et al. (2018) employed density functional theory (DFT) calculation to predict and assign THz vibrational modes related to intermolecular hydrogen bonds found in crystalline urea. Though the material model investigated here was amorphous polyurea, the comparable THz spectral features found in both studies are corroborated by the similarity between the two forms of urea-based structures, namely, inter urea-linkage hydrogen bonds. For instance, Zhao et al. (2018) concluded that the molecular

motions found at 0.66 and 1.06 THz in crystal urea, were assigned to bending and twisting, respectively, of urea molecules bound by a hydrogen bond. Here, the polyurea subjected to shock waves exhibited spectral deviations at comparable frequencies, 0.70–0.73 THz and 0.98–1.02 THz. Since the chemical composition of amorphous polyurea is more convoluted than that of crystalline urea, the slight departure of the spectral amplitude of the former from the DFT calculations done for the latter is anticipated as vibrational modes in polyurea are likely to be coupled to neighboring molecular motions. It should be noted that the polyurea THz spectral features highlighted in Fig. 6 are in great agreement with our previous research (Huynh et al., 2022; Huynh and Youssef, 2021).

The complementary finite element analysis assisted in probing the levels of stress and strain as a function of energy fluence used to generate the shock waves (Gamez et al., 2021). As discussed before, the amplitude of stress profile of the reflected tensile wave at the exact depth of failure is used to determine the dynamic tensile strength of the material (Youssef and Gupta, 2012; Youssef et al., 2012), which is used in conjunction with the SEM micrographs discussed next to determine the polyurea dynamic capacity. Fig. 7a summarizes the solid mechanics results from the FEA simulation, including deviatoric and volumetric strains as well as the true axial stress contours for shock loading at an energy fluence of 995 mJ/mm<sup>2</sup> at 770 ns, when the returning tensile wave trespassed a failure location identified by the scanning electron microscope. The deviatoric normal and shear strain distribution elucidate the dynamic behavior of polyurea as the shock waves plow through the sample structure, including the effect of acoustic impedance mismatch. The mismatch is specifically evident at the interface separating the steel substrate and the polyurea sample, exemplified by shear strain localization. The volumetric strains were at higher levels as their deviatoric counterparts, demonstrating the high hydrostatic effect of the shock wave on polyurea motivated by its incompressible attribute and intensity of propagating stress wave. The dichotomy between the deviatoric and volumetric strains indicate that structural elastoplastic deformations discussed above were hydrostatically dominated. Fig. 7a also includes the true axial stress showing measurable stresses developing in polyurea despite the drastic acoustic impedance mismatch with the steel substrate. The significant volumetric strains and under the assumption of conservation of mass since failure never resulted in material ejection, the third strain invariant (Jacobian) can be related to change in the density, i.e.,  $J \propto \Delta \rho$ . The latter is also associated with changes in the refractive index (n), as described by Gladstone-Dale law,  $\frac{n-1}{2} = \kappa$ , where  $\kappa$  is a constant dependent on atomic and molecular structure of unit volume in the materials under investigation. Concurrently, Eqn. (4) suggests that the changes in the refractive index are proportional to the ratio between the delays (reported in Fig. 5a) and the shock-induced strains deduced from the finite element simulation, i.e.,  $\Delta n \propto \delta/\epsilon_a$ . Fig. 7b shows the correlation between the changes in the Jacobian and refractive index as a function of the energy fluence, signifying possible inflection point in the decrease in the index as the density continued to evolve. In general, the spectroscopic and gravimetric changes ascertain the effect of shocking loading on the conformation of polyurea macromolecule.

The finite element simulation also reported the interrelationship between the free surface displacement and velocity as a function of the illumination energy. Fig. 7c shows the displacement and velocity at the probe location indicated in Fig. 3a at three energy fluences,

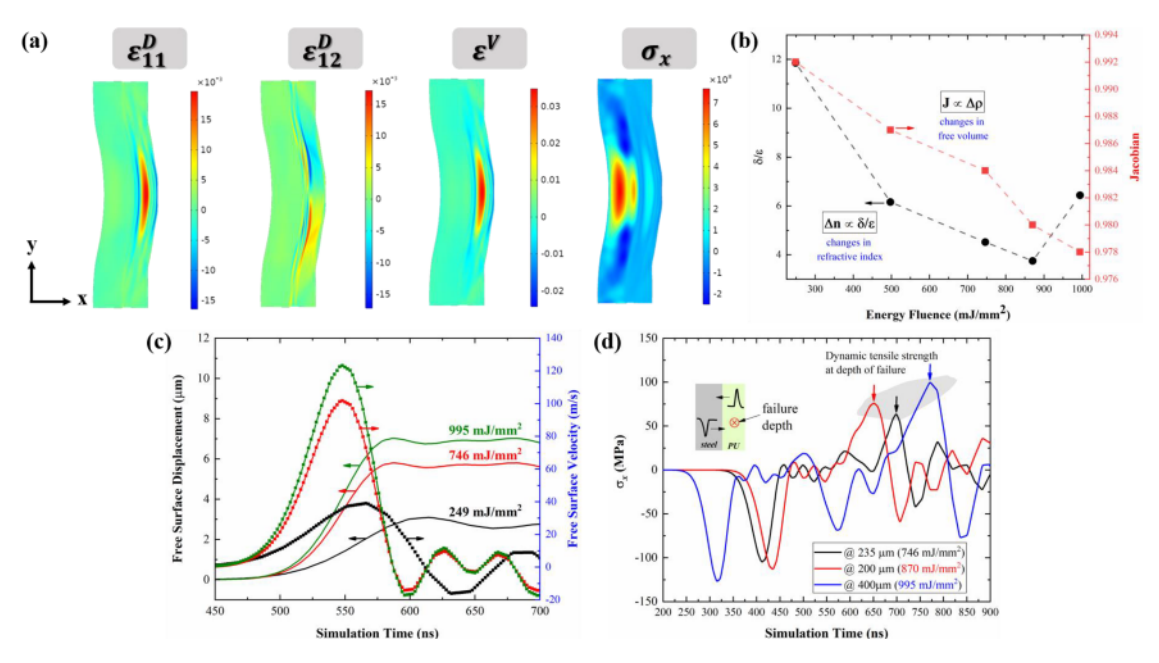


Fig. 7. (a) Finite element results of strain components at an energy fluence of 995 mJ/mm<sup>2</sup>, including normal and shear deviatoric strains ( $\varepsilon_{11}^{D}$ ) and volumetric strain ( $\varepsilon^{V}$ ) as well as the axial true stress ( $\sigma_{x}$ ) at 770 ns, (b) weak correlation between anticipated change in the refractive index and free volume due to compression during shock propagation, (c) comparison of the free surface displacement and velocity at three energy fluences representing low (249 mJ/mm<sup>2</sup>), medium (746 mJ/mm<sup>2</sup>), and high (995 mJ/mm<sup>2</sup>) levels of laser illumination, and (d) normal stress profiles at energy fluences corresponding to the failure modes and depths captured by the scanning electron microscope shown in Fig. 8.

namely 249, 746 and 995 mJ/mm², spanning over the range of fluences investigated herein. This highlights the imperative complementary aspect of FEA in this investigation since the current experimental investigation prevented the concurrent interferometric measurements of free surface displacement or velocity. The computational results are in excellent agreement with previous experimentally measured displacement and velocity in laser-induced shock wave scenarios, e.g., Youssef and Gupta (2012), Huynh et al. (2022), Youssef et al. (2012). Finally, the true axial stresses were extracted and plotted in Fig. 7d for shock-loadings at energy fluences of 746, 870, and 995 mJ/mm² at their respective depths of failure determined using SEM, as discussed next. The peak of the returning tensile wave is taken to be the dynamic strength of polyurea, which ranges between ~ 64–97 MPa, depending on the failure mode, failure depth, and energy fluence. The strength range centers around the values reported before for polyurea under high strain rate testing conditions (Youssef and Gupta, 2012; Jiao et al., 2007), while noting the differences in failure modes and conditions surrounding the loading scenarios. At higher energy fluence, the failure behavior evolved to crazing and vitrification, as discussed next.

Fig. 8 shows three scanning electron micrographs of shock-loaded polyurea elastomers at different energy fluences, elucidating varying degrees of mechanical failure and morphological changes. Fig. 8a displays the initiation of deep cracks into the polyurea plug loaded at an energy fluence of 746 mJ/mm<sup>2</sup> using laser-induced shock waves. The cracks appeared to be nearly parallel to the free surface of the polyurea sample at a depth of ~235 µm, representing the initiation of a spall plane due to the reflected tensile stress wave. Using the results of FEA simulations listed above, this depth corresponds to 63.5 MPa tensile stress, which is below the previously reported dynamic strength of polyurea listed in (Youssef and Gupta, 2012; Jiao et al., 2007) but occurred deeper into the material than the partial spallation strength in Youssef and Gupta (2012) at 153 µm. It should be noted that the current simulation reports 112 MPa at the depth reported by Youssef et al., demonstrating good agreement between the two studies (Youssef and Gupta, 2012). The disparity is attributed to the difference in the loading energy fluence, samples thickness, and depth of failure between the previous results and those reported herein. Nonetheless, future work will focus on performing interferometric measurements at each energy fluence, which will be used to resolve the input stress profile instead of the idealized counterpart used in this research. Fig. 8b is an SEM micrograph of a crack network throughout polyurea with higher distribution close to the free surface when loaded at 870 mJ/mm<sup>2</sup> fluence. Notably, the increased energy fluence implies higher stress levels within the loaded spot, giving rise to enhanced volumetric deformations associated with crazing. The ubiquity of the cracks close to the free surface exemplifies the intensity of the laser-induced shock wave, loading the material at an high strain rate  $> 10^5 \, \mathrm{s}^{-1}$  (based on the velocity plots, v(t), presented in Fig. 7c and the thickness, d, of the samples,  $\dot{\varepsilon} = v(t)/d$ ). The cracks embodied in the sample shown in Fig. 8b most likely manifested during the propagation of the initial compressive wave, given their obliquing angles from the free surface, indicating failure due to shear stresses accompanying the compressive wave. This is further substantiated based on the FEA results discussed above, showing the comparable levels of volumetric and deviatoric strains, where the inception of microcracks (e.g., during crazing) were previously associated with volumetric deformations (Argon, 2013; Youssef, 2021). Finally, Fig. 8c shows morphological changes, signifying localized embrittlement (i.e., vitrification or rubber-to-glass transition) of polyurea due to the high-intensity shock wave at an energy fluence of 995 mJ/mm<sup>2</sup>. Notably, terahertz results at this energy fluence exhibited several spectra changes, including combined or individual peak enhancement, shift, manifestation, and concealment. Therefore, the detection of structural changes from the nondestructive terahertz spectroscopy coincided with the revelation of morphological variations from the destructive SEM investigation, further illustrating the scientific potential of the demonstrated integrated spectro-mechanical experimental setup.

## 5. Conclusion

In closing, this research demonstrates the scientific feasibility of concurrent spectro-mechanical characterization of elastomers submitted to shock loading. Terahertz time-domain spectroscopy, configured in the right-angle reflection mode, was synchronized in real-time with a laser-induced shock wave experimental setup using the firing command simultaneous to the illumination release of a high-energy laser. Stainless-steel/polyurea bilayer sample structures were loaded at eight energy fluences, ranging between 249 and 1119 mJ/mm², by adjusting the illumination energy while maintaining a nanosecond exposure duration. The laser energy exfoliated the silver sacrificial layer, generating a compressive stress wave toward the bilayer sample structure. The spectro-mechanical measurements were followed by electron microscopy observations of the shock-loaded cross-sections and supplemented with finite element analysis of the stress and strain states due to shock propagation. Time and frequency domain analyses of the terahertz data

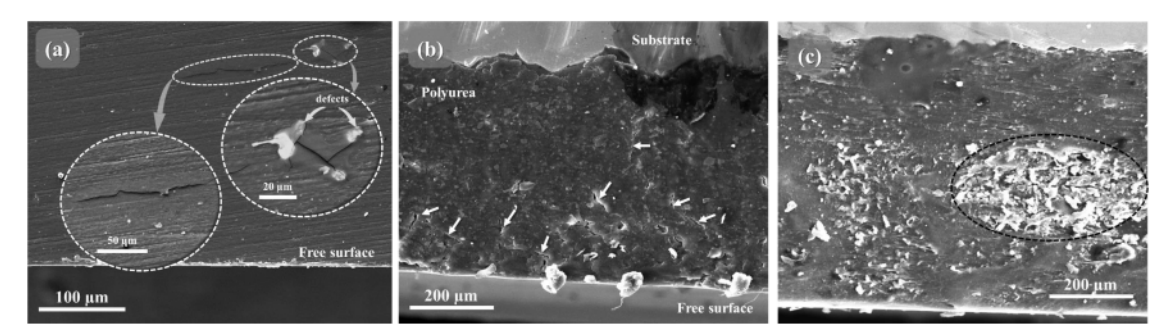


Fig. 8. SEM micrographs of shock-loaded polyurea at (a) 746 mJ/mm<sup>2</sup> showing internal crack initiation, (b) 870 mJ/mm<sup>2</sup> illustrating cracking network close to the free surface, and (c) 995 mJ/mm<sup>2</sup> displaying morphological changes (evidence of vitrification).

revealed spectral changes accompanying the stress wave propagation and rapid recovery after post-loading relaxation. The spectral changes indicate conformational changes in the shock-loaded macromolecule, exemplified by spectral peak shifting, enhancement, manifestation, and concealment, the majority of which were a hallmark of loading at high energy fluences. Temporal and spectral comparisons between unloaded and post-loaded samples indicated that shock loading resulted in elastoplastic deformation and conformation evolution. Electron microscopy observation corroborated some of the terahertz-detected changes while exposing subsurface mechanical failures, including spall and volumetric cracking, as well as morphological changes. Finite element results reported the stress level at a depth of failure. They were used to correlate the Jacobian, a measure of density change, with predicted evolution in the refractive index. In all, this research unlocks the potential for in-depth experimental solid mechanics of the plasticity of elastomers at high strain rate loading while enabling spectro-mechanical characterization.

#### CRediT authorship contribution statement

Nha Uyen Huynh: Methodology, Formal analysis, Investigation, Data curation, Writing – original draft, Writing – review & editing, Visualization, Project administration. George Youssef: Formal analysis, Data curation, Writing – original draft, Writing – review & editing, Supervision, Project administration, Funding acquisition.

## **Declaration of Competing Interest**

The authors declare that they have no known competing financial interests or personal relationships that could have appeared to influence the work reported in this paper.

#### Data availability

Data will be made available on request.

## Acknowledgment

The research leading to these results was supported in part by the United States Department of Defense under Grant Agreement Nos. W911NF1410039 and W911NF1810477. The National Science Foundation under Award No. 1925539 also supported the research. The authors are also grateful for internal funding from San Diego State University. The authors also acknowledge the use of equipment at the San Diego State University Electron Microscopy Facility acquired by NSF instrumentation grant DBI-0959908.

#### References

```
Albrecht, A., Liechti, K., Ravi-Chandar, K., 2013. Characterization of the transient response of polyurea. Exp. Mech. 53 (1), 113-122.
Argon, A.S., 2013. The Physics of Deformation and Fracture of Polymers. Cambridge, New York.
Barsoum, R.G.S., 2015. Elastomeric Polymers With High Rate Sensitivity: Applications in Blast, Shockwave, and Penetration Mechanics. William Andrew.
Blourchian, A., et al., 2021. Segmental evolution of ultraviolet weathered polyurea. J. Polym. Res. 28, 1-9.
Bourne, N.K., 2016. On the shock response of polymers to extreme loading. J. Dyn. Behav. Mater. 2 (1), 33-42.
Boyd, J., Korotkova, N., Grady, M., 2019. Adhesion of biofilms on titanium measured by laser-induced spallation. Exp. Mech. 59 (9), 1275-1284.
Boyd, J.D., et al., 2021. Biofilm and cell adhesion strength on dental implant surfaces via the laser spallation technique. Dent. Mater. 37 (1), 48-59.
Boyd, J.D., Grady, M.E., 2020. The effect of surface roughness on laser-induced stress wave propagation. Appl. Phys. Lett. 117 (12), 121601.
Cheng, L., et al., 2022. A novel aging characterization method for silicone rubber based on terahertz absorption spectroscopy. Polym. Test. 115, 107723.
Clifton, R.J., Wang, X., Jiao, T., 2016. A physically-based, quasilinear viscoelasticity model for the dynamic response of polyurea. J. Mech. Phys. Solids 93, 8-15.
Coutaz, J.L., Garet, F., Wallace, V., 2018. Principles of Terahertz time-Domain Spectroscopy. CRC Press.
Ehsani, H., et al., 2021. Evolution of the laser-induced spallation technique in film adhesion measurement. Appl. Mech. Rev. 73 (3), 030802.
Elamin, M., Varga, J., 2020. Plate impact method for shock physics testing. Mater. Sci. Eng. 4 (1), 31-35.
Fadley, C.S., 2010. X-ray photoelectron spectroscopy: progress and perspectives. J. Electron Spectrosc. Relat. Phenom. 178, 2-32.
Field, J.E., et al., 2004. Review of experimental techniques for high rate deformation and shock studies. Int. J. Impact Eng. 30 (7), 725-775.
Gama, B.A., Lopatnikov, S.L., Gillespie Jr, J.W., 2004. Hopkinson bar experimental technique: a critical review. Appl. Mech. Rev. 57 (4), 223-250.
Gamez, C., Huynh, N.U., Youssef, G., 2021. In-silico experimentations of multimode shock response of polyurea. Int. J. Mech. Sci. 204, 106542.
Grady, M.E., et al., 2014a. Shockwave loading of mechanochemically active polymer coatings. ACS Appl. Mater. Interfaces 6 (8), 5350-5355.
Grady, M.E., Geubelle, P.H., Sottos, N.R., 2014b. Interfacial adhesion of photodefinable polyimide films on passivated silicon. Thin. Solid. Films 552, 116-123.
Graziano, A., Titton Dias, O.A., Petel, O., 2021. High-strain-rate mechanical performance of particle-and fiber-reinforced polymer composites measured with split
    Hopkinson bar: a review. Polym. Compos. 42 (10), 4932-4948.
Grujicic, M., et al., 2015. Experimental and computational study of the shearing resistance of polyurea at high pressures and high strain rates. J. Mater. Eng. Perform.
    24 (2), 778-798.
Gupta, V., et al., 1990. Measurement of interface strength by laser-pulse-induced spallation. Mater. Sci. Eng. A 126 (1-2), 105-117.
Gupta, V., et al., 1992. Measurement of interface strength by a laser spallation technique. J. Mech. Phys. Solids 40 (1), 141-180.
Huynh, N., Youssef, G., 2021. Physical evidence of stress-induced conformational changes in polymers. Exp. Mech. 61 (3), 469-481.
Huynh, N.U., Gamez, C., Youssef, G., 2022. Spectro-microscopic characterization of elastomers subjected to laser-induced shock waves. Macromol. Mater. Eng. 307
    (2), 2100506.
Huynh, N.U., Koohbor, B., Youssef, G., 2023. Light-matter interactions revealing load-induced phase mobility in elastomers. Macromol. Rapid Commun. 44 (7),
    e2200725.
Huynh, N.U., Youssef, G., 2022. Ex situ spectroscopic characterization of residual effects of thermomechanical loading on polyurea. J. Eng. Mater. Technol. 144 (3),
```

Jiao, T. and Clifton, R., Measurement of the response of an elastomer at pressures up to 9 GPa and shear-rates of 105-106s-1. in Journal of Physics: Conference Series. 2014. IOP Publishing.

Jiao, T., Clifton, R.J., Grunschel, S.E., 2007. Pressure-sensitivity and tensile strength of an elastomer at high strain rates. In: AIP Conference Proceedings, 955(1). American Institute of Physics, pp. 707-710.

Klöpffer, W., 2012. Introduction to Polymer Spectroscopy, 7. Springer Science & Business Media.

Koenig, J.L., 1984. Fourier transform infrared spectroscopy of polymers. Spectrosc. NMR Fluoresc. FT-IR 87-154.

Lee, J., et al., 2020. Shock wave energy dissipation in catalyst-free poly (dimethylsiloxane) vitrimers, Macromolecules 53 (12), 4741-4747.

Losego, M.D., et al., 2012. Effects of chemical bonding on heat transport across interfaces. Nat. Mater. 11 (6), 502-506.

Malhotra, P., et al., 2021. Dynamic shearing resistance of hydroxyl-terminated polybutadiene (HTPB). J. Appl. Phys. 129 (24), 245901.

Meyers, M.A., 1994. Dynamic Behavior of Materials. John wiley & sons.

Nakamura, H., et al., 2007. A role for proteoglycans in mineralized tissue-titanium adhesion. J. Dent. Res. 86 (2), 147-152.

Navarro, A., et al., 2012. Bacterial biofilm disruption using laser-generated shockwaves. Advanced Biomedical and Clinical Diagnostic Systems X. SPIE.

Nayak, N., et al., 2012. Effect of matrix on the ballistic impact of aramid fabric composite laminates by armor piercing projectiles. Polym. Compos. 33 (3), 443–450. Nüßler, D., Jonuscheit, J., 2021. Terahertz based non-destructive testing (NDT). TM Tech. Mess. 88 (4), 199–210.

Ranby, B., Rabek, J.F., 2012. ESR Spectroscopy in Polymer Research, 1. Springer Science & Business Media.

Ravindran, S., et al., 2020. Mode-I behavior of adhesively bonded composite joints at high loading rates. Compos. Sci. Technol. 198, 108310.

Ravindran, S., Tessema, A., Kidane, A., 2016. Local deformation and failure mechanisms of polymer bonded energetic materials subjected to high strain rate loading. J. Dyn. Behav. Mater. 2 (1), 146–156.

Ravindran, S., Tessema, A., Kidane, A., 2017. Multiscale damage evolution in polymer bonded sugar under dynamic loading. Mech. Mater. 114, 97–106. Ready, J., 1965. Effects due to absorption of laser radiation. J. Appl. Phys. 36 (2), 462–468.

Ready, J.F., 1997. Industrial Applications of Lasers. Elsevier.

Renganathan, P., Duffy, T.S., Gupta, Y.M., 2020. Hugoniot states and optical response of soda lime glass shock compressed to 120 GPa. J. Appl. Phys. 127 (20), 205901.

Rittel, D., Lee, S., Ravichandran, G., 2002. A shear-compression specimen for large strain testing. Exp. Mech. 42 (1), 58-64.

Rostami, A., Rasooli, H., Baghban, H., 2010. Terahertz Technology: Fundamentals and Applications, 77. Springer Science & Business Media.

J. Shim, et al., An understanding of the mechanism that promotes adhesion between roughened titanium implants and mineralized tissue. 2009.

Shukla, A., Ravichandran, G., Rajapakse, Y., 2010. Dynamic Failure of Materials and Structures, 1. Springer.

Siesler, H.W., et al., 2008. Near-Infrared Spectroscopy: Principles, Instruments, Applications. John Wiley & Sons.

Smith, R.M., Arnold, M.A., 2011. Terahertz time-domain spectroscopy of solid samples: principles, applications, and challenges. Appl. Spectrosc. Rev. 46 (8), 636-679.

Srivastava, P., et al., 2021. Stishovite nucleation at low shock pressures in soda-lime glass. Acta Mater. 215, 117124.

Šuštar, V., et al., 2014. Identification of historical polymers using near-infrared spectroscopy. Polym. Degrad. Stab. 107, 341-347.

Wanchoo, P., et al., 2021. Investigations on air and underwater blast mitigation in polymeric composite structures-a review. Compos. Struct. 263, 113530.

Wang, J., Sottos, N.R., Weaver, R.L., 2004. Tensile and mixed-mode strength of a thin film-substrate interface under laser induced pulse loading. J. Mech. Phys. Solids 52 (5), 999–1022.

Wang, J., Weaver, R.L., Sottos, N.R., 2002. A parametric study of laser induced thin film spallation. Exp. Mech. 42 (1), 74-83.

Wang, Q., Chen, Z., Chen, Z., 2013. Design and characteristics of hybrid composite armor subjected to projectile impact. Mater. Des. 46, 634-639.

Weeks, J., Ravichandran, G., 2022a. Effect of topology on transient dynamic and shock response of polymeric lattice structures. J. Dyn. Behav. Mater. 1-21.

Weeks, J.S., Ravichandran, G., 2022b. High strain-rate compression behavior of polymeric rod and plate Kelvin lattice structures. Mech. Mater. 166, 104216.

Youssef, G., et al., 2012. Inter-wafer bonding strength characterization by laser-induced shock waves. J. Appl. Phys. 111 (9), 094902.

Youssef, G., et al., 2013. The influence of laser-induced nanosecond rise-time stress waves on the microstructure and surface chemical activity of single crystal Cu nanopillars. J. Appl. Phys. 113 (8), 084309.

Youssef, G., 2021. Applied Mechanics of Polymers: Properties, Processing, and Behavior. Elsevier.

Youssef, G., Gupta, V., 2012a. Dynamic response of polyurea subjected to nanosecond rise-time stress waves. Mech. Time Depend. Mater. 16 (3), 317–328.

Youssef, G., Gupta, V., 2012b. Dynamic tensile strength of polyurea. J. Mater. Res. 27 (2), 494-499.

Zhao, Y., Li, Z., Liu, J., Hu, C., Zhang, H., Qin, B., Wu, Y., 2018. Intermolecular vibrational modes and H-bond interactions in crystalline urea investigated by terahertz spectroscopy and theoretical calculation. Spectrochim. Acta Part A 189, 528-534.